RSC Advances

PAPER

View Article Online
View Journal | View Issue

Cite this: *RSC Adv.*, 2020, **10**, 45130

Chitosan modified metal–organic frameworks as a promising carrier for oral drug delivery

Li Li,[ab] Shasha Han,[a] Sengqun Zhao,[a] Xurui Li,[a] Bingmi Liu[ab] and Yu Liu*[ab]

Received 4th October 2020
Accepted 27th November 2020

DOI: 10.1039/d0ra08459j

rsc.li/rsc-advances

Metal–organic frameworks (MOFs) are composed of both organic linkers and metallic ions, which have emerged as excellent drug delivery agents for the treatment of cancer and other diseases. Currently, MOF studies are mainly focused on intravenous administration, while studies dedicated to oral administration are relatively scarce. In this study, five MOFs, namely UiO-66, UiO-66-NH_2, UiO-66-COOH, UiO-67 and Zr-NDC, were synthesized, of which Zr-NDC had the largest drug loading capacity for 5-FU. Next, a chitosan (CS) modified Zr-NDC was developed to provide a strong impetus for the oral administration of 5-FU. *In vitro* release experiments of fluorescein isothiocyanate (FITC)-labeled chitosan demonstrated that the cumulative release rates of FITC-labeled chitosan in artificial gastric juice and artificial intestinal fluid were about 20% and 90%, respectively. The *in vitro* drug release profiles showed that under the protection of CS-MOF, the release of 5-FU into an acidic environment was only 20%, but the release in artificial intestinal fluid reached 70%. Pharmacokinetic analysis revealed that the coating of chitosan on the surface of MOFs exerted a controlled drug release effect, and further improved the oral bioavailability of 5-FU. These findings suggest that CS coating can break through the limitation of MOF intolerance to acid. It is expected that CS-MOF@5-FU can serve as a potential drug delivery system for the oral administration of 5-FU.

1 Introduction

Metal–organic frameworks (MOFs) are constructed from organic bridging ligands and metal nodes.[1] Nowadays, MOFs have attracted increasing attention from researchers due to their facile functionalization, tunable pore sizes and high surface area.[2] These advantageous properties made MOFs promising candidates in many applications, such as gas separation and storage,[3,4] fuel cells,[5] solar cells,[6] catalysis,[7] sensors,[8] electronic devices,[9] drug delivery,[10] and others. In 2008, Férey and co-workers first stated that MOFs had a great potential for drug delivery.[11] As MOFs combined the properties of biodegradability and compatibility, tailorable composition and structure, suitable pore sizes, high drug loading capacity and surface functionalization, they possess great potential as controlled drug delivery systems.[2,12] Currently, MOF studies are mainly focused on intravenous administration,[13–16] while studies dedicated to oral administration are relatively scarce.[17]

For cancer patients, oral chemotherapy is an ideal long-term alternative treatment, since it can maintain appropriate drug concentration in the circulation to prolong the therapeutic effect,[18] reduce side effects and prevent injection discomfort.[19,20] Due to the advantageous features of safeness, high compliance and cost-effectiveness, oral route has been recognized as one of the most common and traditional ways for oral drug delivery.[21] However, the oral delivery of anticancer drugs still faces huge challenges owing to their poor stability in gastrointestinal tract and pre-systemic metabolism. To overcome these limitations, oral drug delivery carriers are being developed to promote drugs to penetrate the mucus barrier[22] and protect the loaded drugs from damage when passing through gastric acid barrier.[18] MOFs are prone to collapse in the environment of gastric acid, which limits their application in oral drug delivery. Therefore, post-synthetic modification of MOFs can serve as a good option to achieve this purpose.

Chitosan (CS) is obtained from the deacetylation of chitin *via* alkaline hydrolysis.[23] CS is a biodegradable, biocompatible and nontoxic biopolymer, with high structural stability.[24] Therefore, modifying the surface of drug carriers with CS can provide many advantages, for example: (i) enhance mucoadhesiveness and tissue penetration, (ii) regulate cell interactions (cellular uptake and toxicity), and (iii) improve oral bioavailability and drug efficacy.[25] At present, one of the most widely studied characteristics of CS is the adhesion ability. Thus, it is speculated that CS-modified MOFs can pass through the gastrointestinal tract. Compared with the pure MOF, CS-coated MOFs maintain their crystalline structure and high porous nature without causing toxicity problems.[26] Surface modification may also enhance the chemical stability and colloidal stability of MOFs in physiological media. CS can improve the stability of MOFs to various

[a]School of Pharmacy, Liaoning University, Shenyang, 110036, China. E-mail: lily63k@163.com
[b]Judicial Expertise Center, Liaoning University, Shenyang, 110036, China

enzymes, while improving the bioadhesive properties and reducing unwanted immune responses. All these characteristics make CS-coated MOF a very promising candidate carrier for oral antitumor drugs.

5-FU is one of the most commonly researched and used drugs to treat various types of cancer, including breast cancer, colorectal cancer and aerodigestive tract cancer.[27] The cytotoxic mechanism of 5-FU is owing to the misincorporation of fluorine nucleotides into RNA and DNA, thereby inhibiting the activity of nucleotide synthase.[28]

In this study, we synthesized five different MOFs and employed 5-FU as a model drug. Then, we selected MOF with the largest drug loading capacity as an optimal carrier. The surface modification of MOFs with CS could not only improve the stability of CS-MOF@5-FU in the gastrointestinal tract, but also increase the permeability of 5-FU across the intestinal mucosa and enhance the oral bioavailability of the drug.

2 Materials and methods

2.1 Materials

2-Aminobenzenedicarboxylic acid (H_2BDC), terephthalic acid, 1,2,4-benzene tricarboxylic acid, zirconium tetrachloride ($ZrCl_4$), 2,6-naphthalene dicarboxylic acid (NDC), and 4,4′-biphenyldicarboxylic acid (BDPC) were obtained from Aladdin reagents Co. Ltd. (Shanghai, China). Acetic acid was from Dingguo Changsheng Biotechnology Co. Ltd. (Beijing, China). All the solvents and reagents used in this study were of analytical grade without any further purification.

2.2 Animals

Male SD mice were purchased from Changsheng Biotechnology Co., Ltd. (Liaoning, China), and used to evaluate the pharmacokinetics of the drug-loaded MOFs. Standard mouse food and water were supplied ad libitum. All animal experiments were carried out according to the ethical principles and guidelines for the use of laboratory animals in research.

2.3 Preparation of five MOFs

2.3.1 Synthesis of UiO-66. A 250 mL round-bottom flask was charged with terephthalic acid (0.897 g), $ZrCl_4$ (1.0036 g), DMF (67 mL), and acetic acid (29 mL). After dissolving, 5 mL of demineralized water was added into the solution, followed by incubation at 120 °C for 15 min. Subsequently, MOFs were separated from the reaction solution by centrifugation (10 000 rpm, 5 min × 3) and washing with methanol. Finally, the drying process was carried out under vacuum at 55 °C, and UiO-66 was obtained.

2.3.2 Synthesis of UiO-66-NH_2. UiO-66-NH_2 was prepared in the light of the synthetic procedure of UiO-66 with slight modification. For example, terephthalic acid was replaced by H_2BDC.

2.3.3 Synthesis of UiO-67. $ZrCl_4$ (0.12 g) and benzoic acid (0.674 g) were dissolved in 20 mL of DMF. Meanwhile, in a second vessel, 0.13 g of BDPC was dissolved in 20 mL of DMF. The two solutions were transferred into a Teflon lined stainless steel hydrothermal autoclave, and 0.028 mL of demineralized water was added. This mixture was sonicated for 10 min, and the reaction was carried out at 120 °C for 24 h. After cooling to room temperature, the product was separated from reaction solution by centrifugation (10 000 rpm, 5 min) and washing one time with DMF and another three times with ethanol. The drying process was carried out under vacuum at 55 °C, and UiO-67 was obtained.

2.3.4 Synthesis of UiO-66-COOH. A 100 mL reaction kettle was charged with 1,2,4-benzene tricarboxylic acid (0.424 g), $ZrCl_4$ (0.463 g), DMF (10 mL), demineralized water (8.8 mL) and acetic acid (12.5 mL). The reaction was carried out at 100 °C for 24 h. Subsequent steps were performed as described in 2.3.3, and UiO-66-COOH was obtained.

2.3.5 Synthesis of Zr-NDC. NDC (0.368 g) and $ZrCl_4$ (0.4 g) were respectively dissolved in 20 mL of DMF by sonication. After properly mixing these two solutions, 2.85 mL of acetic acid and 0.125 mL of deionized water were added and mixed again. The mixture was then sonicated for 30 min at 50–60 °C, and then placed into a hydrothermal autoclave. The reaction was carried out at 120 °C for 24 h. Subsequent steps were performed as described in 2.3.3, and Zr-NDC was obtained.

2.4 Characterization of five MOFs

2.4.1 Fourier transform infrared (FT-IR) and differential scanning calorimetry (DSC) analysis. The five synthesized MOFs were analyzed by FT-IR spectroscopy (Affinity-1, Shimadzu, Tokyo, Japan). DSC thermograms were obtained using (Mettler Toledo, Changzhou, China) DSC system. The MOFs materials were heated from 20 to 400 °C at 10 °C min^{-1} rate.

2.4.2 Morphology and crystal forms. The morphological features of the synthesized MOFs were examined using a scanning electron microscopy (SEM; JSM6510LV, JEOL, Tokyo, Japan). Meanwhile, the crystallinity of the synthesized MOFs was analyzed using an X-ray diffractometer (Bruker, SJC, Beijing, China).

2.5 Loading of 5-FU into the five MOFs

5-Fluorouracil (5-FU) was selected as the model drug, and the carrier with the highest loading capacity of 5-FU was subjected to further analysis. 5-FU (20 mg) and MOFs (10 mg) in 10 mL of ethanol were dispersed by sonication and stirred at 25 °C for 6 h. Then, solvent removal was performed under reduced pressure, and the obtained products were washed with ethanol for three times. The drug-loading efficiency of MOFs was determined by high performance liquid chromatography (HPLC; Agilent LC-20AT).

2.6 Preparation of CS-coated Zr-NDC

Zr-NDC (30 mg) was dissolved in 8.6 mL of ethanol, while CS (10, 20, 30, and 40 mg) was dissolved in 10 mL of aqueous solution containing 0.2% acetic acid under stirring condition for overnight. After that, the above two solutions were mixed and stirred at room temperature for 30 min. In order to remove the excess CS, the obtained product was separated by centrifugation (10 000 rpm, 5 min), and then washed with 1% acetic

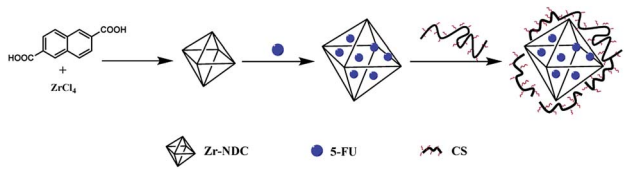

Scheme 1 Synthesis of CS-MOF@5-FU.

acid solution for one time and demineralized water for three times. CS-coated Zr-NDC (hereinafter referred to as "CS-MOF") was obtained by lyophilized for 24 h. The composition route was shown in Scheme 1.

2.7 Characterization of CS-MOF

2.7.1 Ultraviolet spectroscopy (UV) and FT-IR characterization. UV-vis absorption spectral analysis was conducted at room temperature on a UV-2550 spectrophotometer (Shimadzu, Japan). CS, Zr-NDC and CS-MOF samples were analyzed by FT-IR spectroscopy. Measurements were carried out in a spectrum range of 4000–400 cm^{-1} using the KBr pellet method.

2.7.2 Zeta potential, thermogravimetric analysis (TGA) and X-ray diffraction (XRD) characterization. Zeta potential of the blank Zr-NDC and CS-MOF was measured by Zeta sizer Nano ZS (Malvern, UK) at 25 °C. TGA was carried out for CS, Zr-NDC and CS-MOF, with aluminum crucibles as a sample holder under a nitrogen atmosphere. The temperature was elevated from ambient temperature to 700 °C with a heating rate of 10 °C min^{-1}. XRD patterns of the products were recorded on a BrukerD8 Advance X-ray diffractmeter. The patterns were collected at a scanning rate of 5° min^{-1} over a 2θ range from 5° to 45°.

2.7.3 SEM. The morphology of CS-MOF was examined using SEM. A small amount of CS-MOF was dissolved in 5 mL of absolute ethanol solution, dispersed by ultrasound, dropped on a silicon wafer, and placed into a constant-temperature drying oven at 70 °C overnight. After the sample was negatively stained with 2% phosphotungstic acid, its surface structure and morphological features were assessed by a scanning electron microscope.

2.8 *In vitro* release of fluorescein isothiocyanate (FITC)-labeled CS

First, 15 mL of 0.1 M acetic acid was used as a solvent to dissolve 150 mg of CS. Then, 15 mL of methanol was slowly added to the CS solution under continuous stirring. FITC was dissolved in methanol at a concentration of 1.0 mg mL^{-1}, and then slowly added to the CS solution. The reaction was carried out at room temperature for 12 h in the dark. FITC-labeled CS was precipitated in 0.1 M sodium hydroxide solution. The precipitate was rinsed thoroughly with deionized or distilled water until there was a complete absence of free FITC fluorescence signals in the washing medium. Finally, the labeled polymer was frozen dried and stored until further use.

Thereafter, 6 mg of FITC-labeled CS and 6 mL of 0.1 M acetic acid were added into a 10 mL centrifuge tube. After dissolution, a small volume of the diluted solution was taken and then measured with a microplate reader. The labeling rates of CS were calculated according to the following formula.

$$\text{CS labeling rate} = \frac{\text{measuring value}}{\text{theoretical value}} \times 100\%$$

After that, 4 mg of FITC-labeled CS was added into a 6-well culture plate, and 4 mL of artificial gastric juice was then added. The 6-well plate was placed in a constant-temperature shaking incubator (100 rpm, 37 °C). At predetermined time intervals (0.5, 1, 3, 4, 6, 12, 24, 48, and 72 h), 200 μL of the medium was collected and measured prior to data calculation.

All the precursors of the release of FITC-labeled CS in the artificial intestinal fluid were taken as described above. The only difference is that the release medium was changed to artificial intestinal fluid (4 mL).

2.9 *In vitro* drug release experiments of 5-FU-loaded MOFs

The drug-releasing properties of Zr-NDC and CS-MOF loaded with 5-FU (hereinafter referred to as "MOF@5-FU" and "CS-MOF@5-FU", respectively) were evaluated by means of dialysis. Briefly, MOF@5-FU and CS-MOF@5-FU were transferred in dialysis bags and then dialyzed against artificial gastric juice at 37 °C in an air-bath shaker under stirring at 120 rpm. At predetermined time intervals (10, 20, 30 min, 1, 2, 4, 8, 12, 24, 36, 48, 60, and 72 h), 0.5 mL of the medium was collected and replaced with an equal volume of fresh medium. HPLC was used to measure the content of 5-FU released in the solution. The efficiency of 5-FU loading was calculated as follows:

$$Q\% = \left(V_0\, C_t + V \sum_{n-1}^{t-1} C_t \right) 100\% W^{-1}$$

where C_t (mg mL^{-1}) is the drug concentration in the release medium measured at each time point, W (mg) is the total amount of the drug, V_0 is the total volume of the release medium, and V is the volume of each sample.

Then, the release of the drug in the artificial intestinal fluid was similar as above, except that the release medium was changed.

2.10 Pharmacokinetic experiments in rats

All animal procedures were performed in accordance with the Guidelines for Care and Use of Laboratory Animals of Liaoning University and approved by the Animal Ethics Committee of Liaoning University.

The SD mice (200 ± 20 g) were randomly divided into 3 groups ($n = 6$ per group). The rats were fasted for 12 h before this experiment. All the three groups were respectively given 5-FU solution, MOF@5-FU solution, and CS-MOF@5-FU solution *via* oral gavage, with the same 5-FU dose of 50 mg kg^{-1}. Blood samples were collected at the preset time intervals (0.25, 0.5, 1, 2, 4, 6, 8, 10, 12, 24, and 48 h), and subsequently centrifuged at 10 000 rpm for 5 min. The plasma samples were stored at 4 °C for further analysis, and the concentration of 5-FU in plasma was determined by HPLC.

2.11 Statistic analyses

All experimental data were expressed as mean ± standard deviation (SD) in tables and figures. Pharmacokinetic parameters were analyzed using Drug and Statistics (DAS) 2.0 software. Student's *t* test was used to compare the differences between groups. *P*-Values < 0.05 were regarded as statistically significant.

3 Results and discussion

3.1 Characterization of the five MOFs

3.1.1 FT-IR data. FT-IR spectroscopy was employed to deeply understand the molecular structure of MOF materials. Fig. 1a shows the IR spectra of UiO-66 (black curve), UiO-66-NH_2 (red curve), UiO-66-COOH (blue curve), UiO-67 (pink curve) and Zr-NDC (yellow curve). The absorption band at 744 cm^{-1} was attributed to the C–H bonding vibration of the benzene rings. Additionally, a broad peak at 3700–3000 cm^{-1} was assigned to the terminal hydroxyl group of MOFs. The peaks at 1640 and 1373 cm^{-1} were ascribed to the asymmetric and symmetric vibration of the OCO group, respectively, while the peak at 1652 cm^{-1} represented the C=O stretching vibration. For UiO-66-NH_2, the peaks at 1655–1590 cm^{-1} were due to N–H bonds.

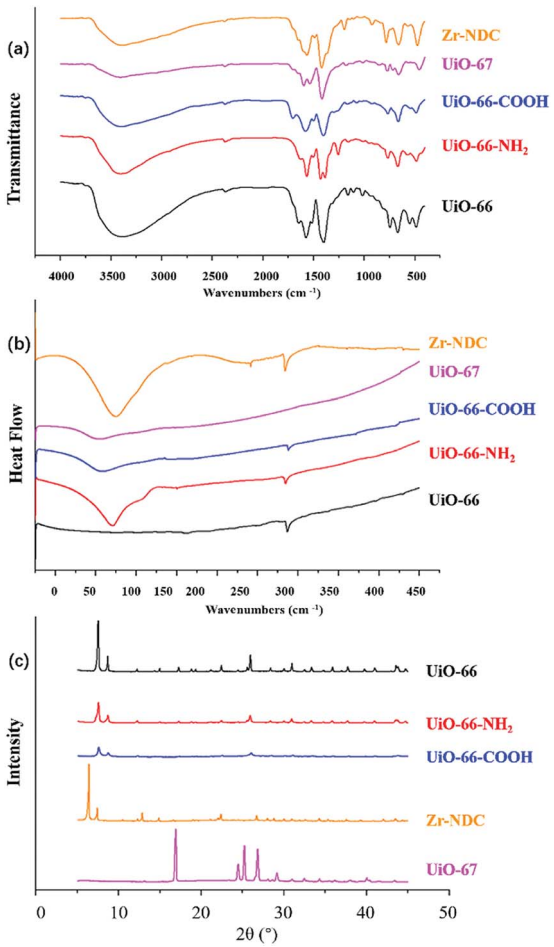

Fig. 1 Infrared spectra (a), DSC diagram (b) and XRD diagram (c) of five MOFs.

3.1.2 DSC patterns. DSC was conducted to investigate the crystalline state of the five MOFs. The DSC curves of the five MOFs are shown in Fig. 1b. Notably, an endothermic peak centered around 75 °C was observed, which could be attributed to absolute ethyl alcohol. Moreover, the five MOFs did not fluctuate significantly within the range of −25 °C to 450 °C, indicating that all the MOFs are heat-stable carriers.

3.1.3 Morphology and crystal forms. SEM was used to assess the morphology and particle size of the five MOFs, as shown in Fig. 2a–e. It was observed that the morphological features of the five MOFs were relatively similar, *i.e.*, regular octahedron in shape. The average diameter of Zr-NDC was determined to be 800 nm, which appeared larger than the others.

XRD was a useful technique for the investigation of crystalline properties in the synthetic MOFs. The XRD patterns of UiO-66, UiO-66-NH_2, UiO-66-COOH, UiO-67 and Zr-NDC in the 2θ range of 5°–45° are shown in Fig. 1c. Obviously, the diffraction of UiO-66 fits well with the diffraction patterns reported in previous literature.[29,30] The main peaks of UiO-66-NH_2 and UiO-66-COOH were comparable with UiO-66, revealing that the introduction of NH_2 or COOH groups did not change the crystal structure of matrix UiO-66. These results were consistent with those of previous studies.[31–33] In addition, the XRD patterns of UiO-67 and Zr-NDC differed greatly from those of the other three MOFs, mainly due to the large difference in organic ligands.

3.2 Screening of the optimal carrier

As can be seen from Table 1, the encapsulation rates of the five MOFs were ranked as follows: Zr-NDC > UiO-66-NH_2 > UiO-66-COOH > UiO-67 ≈ UiO-66. Compared with UiO-66, the encapsulation rate of UiO-67 did not change remarkably, while UiO-66-NH_2 and UiO-66-COOH exhibited an improved encapsulation rate. Given that the structure and pore size of MOFs can be tuned by functionalizing the organic linkers with groups such as –COOH, –NH_2,[34] the encapsulation rate is capable of being changed accordingly. In addition, as the organic ligand chain was increased and retained more drugs, the encapsulation rate and drug loading of Zr-NDC were significantly increased, reaching as high as 66.28% and 1.3 g g^{-1}, respectively. Therefore, Zr-NDC was selected as an anticancer drug carrier in subsequent experiments.

SEM was employed to study the structural evolution of the synthesized Zr-NDC before and after drug loading. As shown in Fig. 2e–f, the morphology for Zr-NDC was regular octahedron

Table 1 Drug loading and encapsulation rates of five MOFs

MOFs	Encapsulation rate (%)	Drug loading (g g^{-1})
UiO-66-COOH	18.71 ± 1.38	0.40 ± 0.03
UiO-66-NH_2	22.49 ± 3.23	0.44 ± 0.06
UiO-66	14.26 ± 2.15	0.28 ± 0.05
UiO-67	14.76 ± 1.22	0.28 ± 0.03
Zr-NDC	66.28 ± 0.01	1.30 ± 0.05

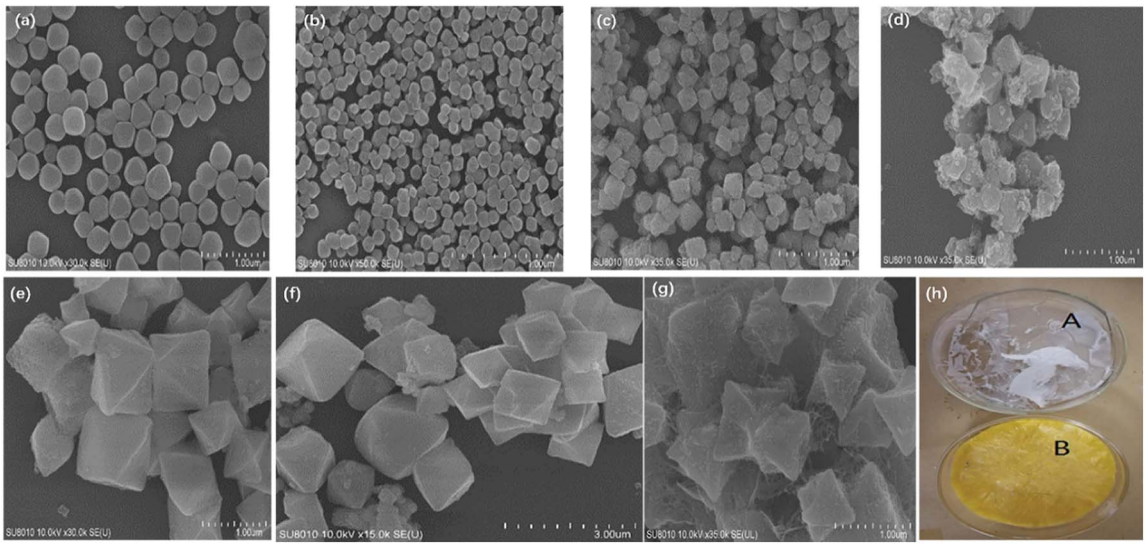

Fig. 2 SEM images of UiO-66 (a), UiO-66-NH_2 (b), UiO-66-COOH (c), UiO-67 (d), Zr-NDC (e), Zr-NDC after drug loading (f) and Zr-NDC coated with CS (g). (h) Appearance of CS and fluorescein isothiocyanate CS.

with an average diameter of 800 nm. By comparing the SEM of 5-FU loaded-MOFs with that of Zr-NDC, it was found that its morphology remained almost the same after drug loading.

3.3 Characterization of CS-MOF

3.3.1 UV spectral characteristics. As shown in Fig. 3a, UV-visible absorption spectrum was used to assess the effects of CS on Zr-NDC. The absorption peak of Zr-NDC was not clearly observed. After the incorporation of CS, a small peak appeared at 240 nm in the spectrum, which was likely derived from CS. Notably, the absorbance spectrum increased gradually with increasing concentrations of CS. This may be due to the existence of acetyl groups on CS, thus resulting in a conjugated absorption. All these results proved that CS was successfully coated on the surface of Zr-NDC.

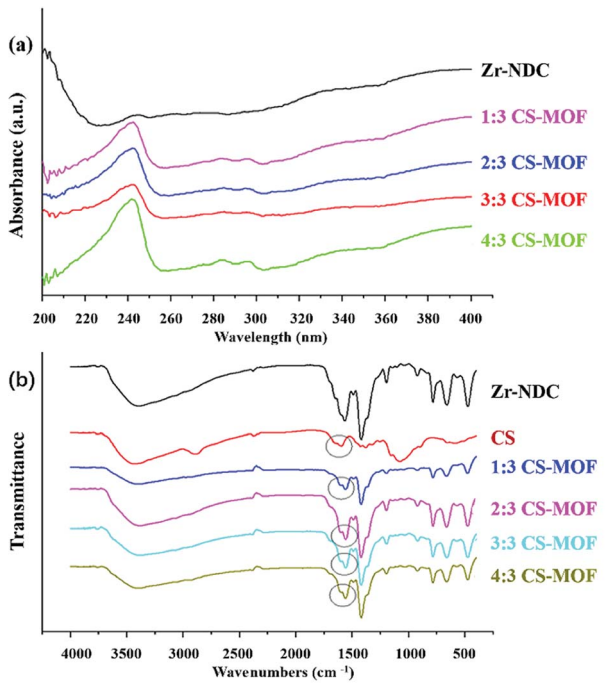

Fig. 3 Uv images (a) and infrared images (b) of Zr-NDC and different proportions of CS coated with Zr-NDC.

3.3.2 FT-IR analysis. FT-IR spectra of the free CS, Zr-NDC and CS-MOF are depicted in Fig. 3b. The peaks of CS were observed at about 3410 cm^{-1} (ν_{O-H} and ν_{N-H}), 1623 and 1513 cm^{-1} (δ_{N-H}), 1088 cm^{-1} (ν_{C-N}), 651 cm^{-1} (δ_{NH_2}), 651 cm^{-1} (due to amino groups) and 895 cm^{-1} (epimeric β–δ_{C-H} of cyclic pyranosyl rings). Zr-NDC exhibited characteristic peaks at the region of 1400–1700 cm^{-1}, which corresponded to the typical vibrational bands of the carboxylic acid function. The characteristic peaks due to the C–H bonding vibration of the benzene rings were found at 747 cm^{-1}. After conjugation of CS to Zr-NDC, the typical bands of CS (1600 cm^{-1}) and Zr-NDC (1400 cm^{-1} and 800–700 cm^{-1}) were all observed in CS-MOF spectra.

Chitosan can be incorporated onto the MOF surfaces *via* adsorption process. In this study, the five MOFs were placed in chitosan dispersion until equilibrium was reached. Mechanistically, this process often takes place in three consecutive steps: diffusion, attachment, and rearrangement/relaxation.[35] Chitosan coating has proven to be useful in modifying the superficial characteristics of MOFs and improve their physicochemical properties.[25]

3.3.3 Zeta potential. Zeta potential is an important characterization method for the chemical modification of MOFs, as the altered surface of MOFs may cause substantial differences in their surface charges.[26] The value of zeta potential represented the degree of electrostatic repulsion or attraction between adjacent particles, implicating that particles with high zeta potential are electrically stable and tend to avoid aggregation.[25] The effect of CS concentration on the ζ-potential of Zr-

Table 2 Zeta potential value of Zr-NDC and different proportions of CS coated with Zr-NDC

MOFs	Zeta potential in water
Zr-NDC	38.37 ± 0.82
1 : 3CS-Zr-NDC	39.43 ± 0.34
2 : 3CS-Zr-NDC	42.00 ± 0.41
3 : 3CS-Zr-NDC	48.50 ± 0.08
4 : 3CS-Zr-NDC	43.82 ± 0.20

NDC was investigated by using Zeta sizer Nano ZS. Table 2 demonstrates the ζ-potential of CS-MOF with different CS concentrations. It was obvious that CS concentration had some influence on the ζ-potential of the prepared CS-MOF. Zeta potential value of bare Zr-NDC was determined to be 38.37 ± 0.82 mv, and that of CS was also positive. Further addition of CS could increase the ζ-potential of CS-MOF. When the ratio of CS to Zr-NDC was 3 : 3, the ζ-potential value was the highest and CS-MOF had the most excellent stability. Then MOFs exhibited reduced surface charges, as the quantity of introduced CS increased. These results indicated that CS could be used to effectively modify the surface of Zr-NDC, and the ratio of 3 : 3 was selected for subsequent experiments.

3.3.4 TGA. The success of surface modification was also confirmed by TGA. As shown in Fig. 4a, the decomposition of CS was observed at 250–450 °C. CS-MOFs also disappeared in the area with a weight reduction of 4.84%. Moreover, the TGA curves of CS-MOF were similar with their parent MOFs, except for larger weight loss area for the loss of modified CS. The increase in weight loss verified the success of surface modification.

3.3.5 XRD. XRD analysis was carried out to investigate the crystalline structures of Zr-NDC, CS and CS-MOF. As shown in Fig. 4b, the characteristic peak of CS was observed at the 2θ of 20°; while the peak positions of CS-MOF and pure Zr-NDC sample were in good agreement with each other, except for a slight decrease in intensity caused by surface modification. These findings revealed that CS was successfully wrapped on the surface of Zr-NDC, without changing the surface structure.

3.3.6 SEM. The morphological features of the synthesized Zr-NDC and CS-MOF were examined by SEM, as shown in Fig. 2g. Without CS modification, the structure of Zr-NDC remained stable. In the presence of CS, the prepared CS-MOF eventually condensed together due to the cohesiveness of CS. This indicates that CS has little effect on the shape of Zr-NDC and confirms the successful functionalization of Zr-NDC surface with CS capping.

3.4 *In vitro* release experiments of FITC-labeled CS

As shown in Fig. 2h, the appearance of CS was white floccus, while that of FITC-labeled CS was golden floccus. The cumulative release rates of FITC-labeled CS in the artificial gastric juice and artificial intestinal fluid were about 20% and 90%, respectively (Fig. 5). The pKa of the primary amine groups of CS was approximately 6.5. The pH-dependent profile of CS could be explained by its stronger charges at lower pH levels, thus increasing the rigidity of CS chains. At intestinal pH levels, CS contained less charged, and the chains had more mobility.[36] Hence, FITC-labeled CS remained intact in the pH environment below 7.0, but became unstable and disintegrated at pH above 7.0.[37] Altogether, FITC-labeled CS showed different cumulative release rates in both artificial gastric juice and artificial intestinal fluid.

3.5 *In vitro* drug release experiments of 5-FU-loaded MOFs

Fig. 6a shows the *in vitro* release profiles of 5-FU-loaded Zr-NDC and CS-MOF in artificial gastric medium. It could be seen that

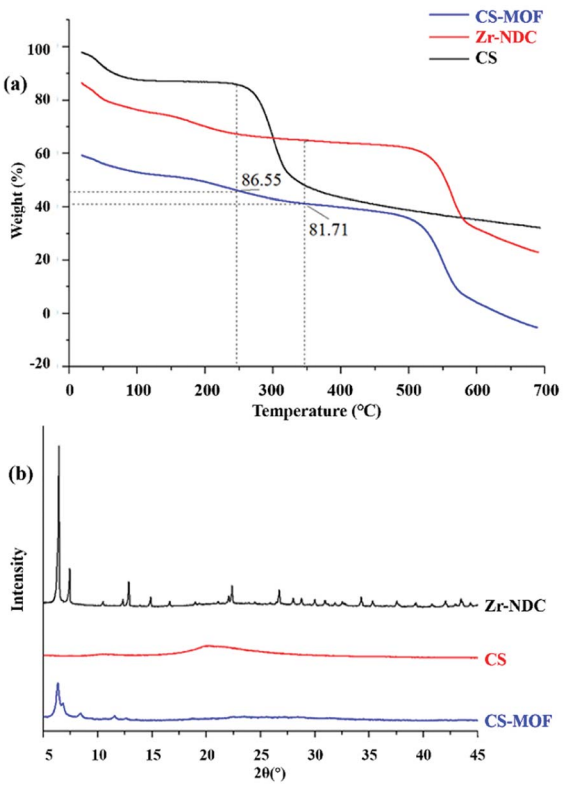

Fig. 4 TGA diagram (a) and XRD patterns (b) of Zr-NDC, CS and CS coated with Zr-NDC.

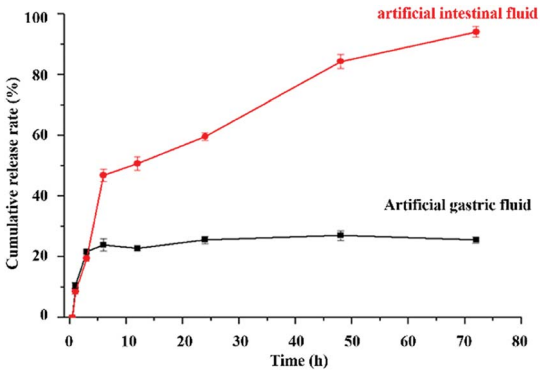

Fig. 5 The release curve of fluorescein isothiocyanate CS.

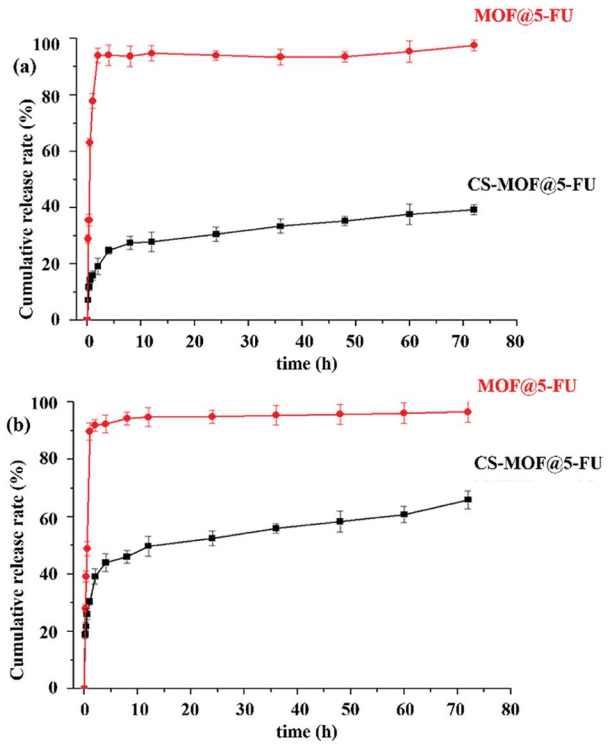

Fig. 6 Drug release in artificial gastric medium (a) and artificial intestinal fluid (b).

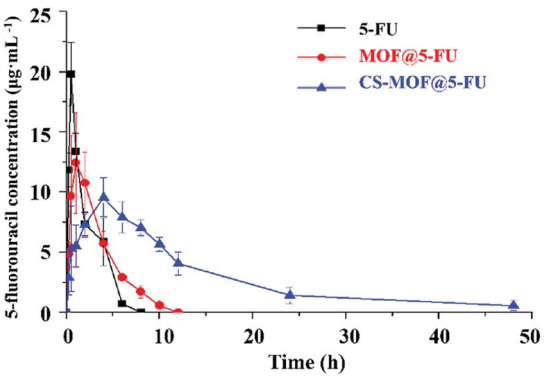

Fig. 7 Blood drug mass concentration-time curve.

Table 3 Pharmacokinetic parameters (n = 6, mean ± SD)

Paramater	5-FU	MOF@5FU	CS-MOF@5FU
$t_{1/2}$/h	1.473 ± 0.449	2.204 ± 0.629	8.643 ± 5.408
T_{max}	0.667 ± 0.289	1.167 ± 0.764	4.667 ± 1.155
C_{max}/μg mL^{-1}	21.041 ± 1.981	15.328 ± 1.677	9.581 ± 1.626
AUC_{0-t}	50.391 ± 10.82	51.764 ± 1.68	135.648 ± 25.488
$AUC_{0-\infty}$	54.564 ± 15.013	55.178 ± 1.297	145.420 ± 26.989

95% of 5-Fu was released from MOF@5-FU within the first 2 h, while the released amount of CS-MOF@5-FU decreased greatly under the same conditions. The pure Zr-NDC was unstable and its structure was destroyed under acidic conditions, leading to the release of most drugs. When CS-MOF was used as a carrier, the drug was slowly released, which could be attributed to the protection of CS coating. These results suggest that the incorporation of CS not only helps to lock the drugs in the frameworks, but also stabilizes the framework structure to prevent the degradation of crystal structure and possible drug leakage.

Fig. 6b shows the *in vitro* release profiles of 5-FU-loaded Zr-NDC and CS-MOF in artificial intestinal fluid. Obviously, 95% of 5-Fu was released from MOF@5-FU within the first 1 h. Under the conditions of alkaline environment and pancreatin, the pure Zr-NDC skeleton collapsed, which in turn increases the amount of drug release. Meanwhile, the amount of 5-Fu released from CS-MOF@5-FU was only 30% under the same conditions and within the same time period. At the end of this experiment, the cumulative amount of 5-Fu released from CS-MOF@5-FU was about 60%. Under the conditions of trypsin and pancreatic lipase, the structure of CS-MOF was gradually destroyed, and the drug was slowly released. Our results indicate that the modification of MOF surfaces turns out to be an effective method to reduce premature drug release.

3.6 Pharmacokinetic studies

The mean plasma concentration-time profiles of 5-FU, MOF@5FU and CS-MOF@5-FU are shown in Fig. 7, and the corresponding pharmacokinetic parameters are summarized in Table 3. As can be seen from Fig. 7, the value of C_{max} reached 20 μg mL^{-1} after 0.5 h of oral 5-FU administration. Moreover, the C_{max} of 5-FU reached 12.5 μg mL^{-1} after 1 h of oral MOF@5-FU administration, and that of 5-FU reached 9 μg mL^{-1} after 4 h of oral CS-MOF@5-FU administration. Besides, the T_{max} of CS-MOF@5-FU was longer than that of 5-FU and MOF@5-FU, but the C_{max} of CS-MOF@5-FU was lower than that of 5-FU and MOF@5-FU, indicating that the drug release is delayed. Therefore, it can be inferred that CS, as a coating material of MOFs, prolongs the release time of drugs and has a controlled drug release effect. As summarized in Table 3, the half-life ($t_{1/2}$) values of CS-MOF@5-FU and MOF@5-FU appeared to be 8.643 ± 5.408 and 2.204 ± 0.629 h, which were 5.87 and 1.50 times longer than that of 5-FU, respectively. The extension of the half-life further indicated the sustained release of the drug carriers. The AUC (area under curve) of CS-MOF@5-FU was determined to be 135.648 ± 25.488, which was 2.69- and 2.62-fold higher than that of 5-FU and MOF@5-FU, respectively. These findings reveal that CS-MOF@5-FU can remarkably improve the oral bioavailability of 5-FU.

4 Conclusions

The nanoscale MOFs UiO-66, UiO-66-NH_2, UiO-66-COOH, UiO-67 and Zr-NDC were successfully synthesized and characterized. Drug loading of MOFs was assessed by utilizing 5-FU as model drug, among which Zr-NDC had the largest drug loading and was selected for further analysis. Next, Zr-NDC was modified with CS, and subsequently characterized by UV, FT-IR, zeta potential, TGA, PXRD and SEM. When the ratio of CS to Zr-NDC

was 3 : 3, the drug carrier was the most superior. Based on the *in vitro* release experiments of FITC-labeled CS, it could be concluded that CS had a certain resistance to artificial gastric juice, but the structure was greatly destroyed by the simultaneous action of trypsin and pancreatic lipase in artificial intestinal fluid. The 5-FU release studies indicated that the pure Zr-NDC was unstable in both artificial gastric juice and artificial intestinal fluid. However, CS coating could increase the stability of MOFs in the acidic solvents and prolong the residence time of MOFs in the intestinal tract, which in turn contributes to the release and absorption of drugs. Pharmacokinetic studies also confirmed that CS modified MOFs could prolong the release time of 5-FU, and thus exerting a controlled drug-release effect. The oral bioavailability of 5-FU could also be enhanced. The obtained results suggest that CS-MOF@5-FU can serve as a potential drug delivery system for the oral administration of 5-FU.

Conflicts of interest

There are no conflicts to declare.

Acknowledgements

The study was supported by the Natural Science Foundation of Liaoning Province (20180510016). We would like to express our gratitude to EditSprings (https://www.editsprings.com/) for the expert linguistic services provided.

Notes and references

1 R. C. Huxford, K. E. deKrafft, W. S. Boyle, D. Liu and W. Lin, Lipid-coated nanoscale coordination polymers for targeted delivery of antifolates to cancer cells, *Chem. Sci.*, 2012, **3**, 198–204.
2 H. P. Nguyen Thi, H. D. Ninh, C. V. Tran, B. T. Le, S. V. Bhosale and D. D. La, Size-Control and Surface Modification of Flexible Metal-Organic Framework MIL-53(Fe) by Polyethylene glycol for 5-Fluorouracil Anticancer, *Drug Delivery*, 2019, **4**, 2333–2338.
3 J. Zheng, X. Cui, Q. Yang, Q. Ren, Y. Yang and H. Xing, Shaping of ultrahigh-loading MOF pellet with a strongly anti-tearing binder for gas separation and storage, *Chem. Eng. J.*, 2018, **354**, 1075–1082.
4 P. Barbosa, L. Cumba, R. Andrade and D. Do Carmo, Chemical Modifications of Cyclodextrin and Chitosan for Biological and Environmental Applications: Metals and Organic Pollutants Adsorption and Removal, *J. Polym. Environ.*, 2019, **27**, 1–15.
5 X. Qin, Y. Huang, K. Wang, T. Xu, Y. Wang, P. Liu, Y. Kang and Y. Zhang, Novel hierarchically porous Ti-MOFs/nitrogen-doped graphene nanocomposite served as high efficient oxygen reduction reaction catalyst for fuel cells application, *Electrochim. Acta*, 2019, **297**, 805–813.
6 R. Kaur, A. L. Sharma, K.-H. Kim and A. Deep, A novel CdTe/Eu-MOF photoanode for application in quantum dot-sensitized solar cell to improve power conversion efficiency, *J. Ind. Eng. Chem.*, 2017, **53**, 77–81.
7 Y. Zhang, X. Yang and H.-C. Zhou, Synthesis of MOFs for heterogeneous catalysis via linker design, *Polyhedron*, 2018, **154**, 189–201.
8 K. Zhan, Y. Zhu, J. Yan and Y. Chen, Enhanced-performance relative humidity sensor based on MOF-801 photonic crystals, *Phys. Lett. A*, 2020, **384**, 126678.
9 Y. Liu, Y. Wang, Y. Chen, C. Wang and L. Guo, NiCo-MOF nanosheets wrapping polypyrrole nanotubes for high-performance supercapacitors, *Appl. Surf. Sci.*, 2020, **507**, 145089.
10 I. Abánades Lázaro and R. S. Forgan, Application of zirconium MOFs in drug delivery and biomedicine, *Coord. Chem. Rev.*, 2019, **380**, 230–259.
11 G. Férey, Hybrid porous solids: past, present, future, *Chem. Soc. Rev.*, 2008, **37**, 191–214.
12 H. Zhang, Y. Shang, Y.-H. Li, S.-K. Sun and X.-B. Yin, Smart Metal–Organic Framework-Based Nanoplatforms for Imaging-Guided Precise Chemotherapy, *ACS Appl. Mater. Interfaces*, 2019, **11**, 1886–1895.
13 L. Li, S. Han, C. Yang, L. Liu, S. Zhao, X. Wang, B. Liu, H. Pan and Y. Liu, Glycyrrhetinic acid modified MOFs for the treatment of liver cancer, *Nanotechnology*, 2020, **31**, 325602.
14 S. Sharma, D. Mittal, A. K. Verma and I. Roy, Copper-Gallic Acid Nanoscale Metal–Organic Framework for Combined Drug Delivery and Photodynamic Therapy, *ACS Appl. Bio Mater.*, 2019, **2**, 2092–2101.
15 X. G. Wang, Z. Y. Dong, H. Cheng, S. S. Wan, W. H. Chen, M. Z. Zou, J. W. Huo, H. X. Deng and X. Z. Zhang, A multifunctional metal-organic framework based tumor targeting drug delivery system for cancer therapy, *Nanoscale*, 2015, **7**, 16061–16070.
16 T. Simon-Yarza, T. Baati, F. Neffati, L. Njim, P. Couvreur, C. Serre, R. Gref, M. F. Najjar, A. Zakhama and P. Horcajada, In vivo behavior of MIL-100 nanoparticles at early times after intravenous administration, *Int. J. Pharm.*, 2016, **511**, 1042–1047.
17 S. Javanbakht, A. Hemmati, H. Namazi and A. Heydari, Carboxymethylcellulose-coated 5-fluorouracil@MOF-5 nano-hybrid as a bio-nanocomposite carrier for the anticancer oral delivery, *Int. J. Biol. Macromol.*, 2020, **155**, 876–882.
18 L. Yin, Z. Meng, Y. Zhang, K. Hu, W. Chen, K. Han, B. Y. Wu, R. You, C. H. Li, Y. Jin and Y. Q. Guan, Bacillus spore-based oral carriers loading curcumin for the therapy of colon cancer, *J. Controlled Release*, 2017, **271**, 31–44.
19 M. Filippousi, S. Turner, K. Leus, P. I. Siafaka, E. D. Tseligka, M. Vandichel, S. G. Nanaki, I. S. Vizirianakis, D. N. Bikiaris, P. Van Der Voort and G. Van Tendeloo, Biocompatible Zr-based nanoscale MOFs coated with modified poly(ε-caprolactone) as anticancer drug carriers, *Int. J. Pharm.*, 2016, **509**, 208–218.
20 S. Javanbakht, P. Nezhad-Mokhtari, A. Shaabani, N. Arsalani and M. Ghorbani, Incorporating Cu-based metal-organic framework/drug nanohybrids into gelatin microsphere for ibuprofen oral delivery, *Mater. Sci. Eng., C*, 2019, **96**, 302–309.

21 K. Thanki, R. P. Gangwal, A. T. Sangamwar and S. Jain, Oral delivery of anticancer drugs: challenges and opportunities, *J. Controlled Release*, 2013, **170**, 15–40.
22 L. M. Ensign, R. Cone and J. Hanes, Oral drug delivery with polymeric nanoparticles: the gastrointestinal mucus barriers, *Adv. Drug Delivery Rev.*, 2012, **64**, 557–570.
23 N. A. Negm, H. H. H. Hefni, A. A. A. Abd-Elaal, E. A. Badr and M. T. H. A. Kana, Advancement on modification of chitosan biopolymer and its potential applications, *Int. J. Biol. Macromol.*, 2020, **152**, 681–702.
24 Z. Khan, Chitosan capped Au@Pd@Ag trimetallic nanoparticles: synthesis, stability, capping action and adsorbing activities, *Int. J. Biol. Macromol.*, 2020, **153**, 545–560.
25 L. A. Frank, G. R. Onzi, A. S. Morawski, A. R. Pohlmann, S. S. Guterres and R. V. Contri, Chitosan as a coating material for nanoparticles intended for biomedical applications, *React. Funct. Polym.*, 2019, **147**, 104459.
26 T. Hidalgo, M. Giménez-Marqués, E. Bellido, J. Avila, M. C. Asensio, F. Salles, M. V. Lozano, M. Guillevic, R. Simón-Vázquez, A. González-Fernández, C. Serre, M. J. Alonso and P. Horcajada, Chitosan-coated mesoporous MIL-100(Fe) nanoparticles as improved bio-compatible oral nanocarriers, *Sci. Rep.*, 2017, **7**, 43099.
27 D. B. Longley, D. P. Harkin and P. G. Johnston, 5-Fluorouracil: mechanisms of action and clinical strategies, *Nat. Rev. Cancer*, 2003, **3**, 330–338.
28 N. Zhang, Y. Yin, S. J. Xu and W. S. Chen, 5-Fluorouracil: Mechanisms of Resistance and Reversal Strategies, *Molecules*, 2008, **13**, 1551–1569.
29 J. H. Cavka, S. Jakobsen, U. Olsbye, N. Guillou, C. Lamberti, S. Bordiga and K. P. Lillerud, A new zirconium inorganic building brick forming metal organic frameworks with exceptional stability, *J. Am. Chem. Soc.*, 2008, **130**, 13850–13851.
30 M. Schelling, M. Kim, E. Otal and J. Hinestroza, Decoration of Cotton Fibers with a Water-Stable Metal-Organic Framework (UiO-66) for the Decomposition and Enhanced Adsorption of Micropollutants in Water, *Bioengineering*, 2018, **5**, 14.
31 S. Ashtiani, M. Khoshnamvand, A. Shaliutina-Kolešová, D. Bouša, Z. Sofer and K. Friess, Co(0·5)Ni(0·5)FeCrO(4) spinel nanoparticles decorated with UiO-66-based metal-organic frameworks grafted onto GO and O-SWCNT for gas adsorption and water purification, *Chemosphere*, 2020, **255**, 126966.
32 Y. Cao, H. Zhang, F. Song, T. Huang, J. Ji, Q. Zhong, W. Chu and Q. Xu, UiO-66-NH_2/GO Composite: Synthesis, Characterization and CO_2 Adsorption Performance, *Materials*, 2018, **11**, 589.
33 N. Zhang, L. Y. Yuan, W. L. Guo, S. Z. Luo, Z. F. Chai and W. Q. Shi, Extending the Use of Highly Porous and Functionalized MOFs to Th(IV) Capture, *ACS Appl. Mater. Interfaces*, 2017, **9**, 25216–25224.
34 W. Chen and C. Wu, Synthesis, functionalization, and applications of metal-organic frameworks in biomedicine, *Dalton Trans.*, 2018, **47**, 2114–2133.
35 M. L. Del Prado-Audelo, I. H. Caballero-Florán, J. Sharifi-Rad, N. Mendoza-Muñoz, M. González-Torres, Z. Urbán-Morlán, B. Florán, H. Cortes and G. Leyva-Gómez, Chitosan-decorated nanoparticles for drug delivery, *J. Drug Delivery Sci. Technol.*, 2020, **59**, 101896.
36 A. Almeida, M. Araújo, R. Novoa-Carballal, F. Andrade, H. Gonçalves, R. L. Reis, M. Lúcio, S. Schwartz Jr and B. Sarmento, Novel amphiphilic chitosan micelles as carriers for hydrophobic anticancer drugs, *Mater. Sci. Eng., C*, 2020, **112**, 110920.
37 L. Liu, H. Yang, Y. Lou, J. Y. Wu, J. Miao, X. Y. Lu and J. Q. Gao, Enhancement of oral bioavailability of salmon calcitonin through chitosan-modified, dual drug-loaded nanoparticles, *Int. J. Pharm.*, 2019, **557**, 170–177.